Received: 23 July 2020 | Revised: 3 December 2020 | Accepted: 6 December 2020

DOI: 10.1002/nag.3181

RESEARCH ARTICLE

WILEY

Time-resolved model for geothermal engineering in high porosity Slochteren sandstone

Aditya Singh[1] | **Peter A. Fokker**[1,2]

[1] HPT lab, Utrecht University, Utrecht, The Netherlands

[2] TNO Applied Geosciences, Utrecht, The Netherlands

Correspondence
Aditya Singh and Peter A. Fokker,
HPT lab, Utrecht University, Utrecht, The Netherlands.
Email: aditya.singh@ce.iitr.ac.in and peter.fokker@tno.nl

Present address: Aditya Singh, Department of Civil Engineering, Indian Institute of Technology, Roorkee 247667, India.

Funding information
European Union's Horizon 2020, Grant/Award Number: 691728

Abstract

This work is an extension of the time-resolved poro-elasto-plastic Mohr-Coulomb model by Fokker et al to include a more realistic constitutive model. Experiments on Slochteren sandstone revealed that the inelastic deformation contributes significantly in compressive deformation almost in all stages of loading and instigated the development of a Cam-Clay-like model to reproduce the Slochteren sandstone behavior. This model was adopted for the current extension. A typical behavior of this model is that the presence of a borehole causes both elastic and inelastic deformation everywhere in the reservoir, as opposed to the conventional philosophy with plastic and elastic zones.

Our solution handles the spatial and temporal evolution of pressures, permeability, elastic and plastic properties under the assumption of symmetric loading. The applicability of the approach is demonstrated through a number of cases, like fluid injection, shut-in, production, stimulation, and an injection-production sequence.

KEYWORDS

circular cavity, geothermal stimulation, injection, poro-elasto-plastic model, production, Slochteren sandstone, wellbore/borehole

1 | INTRODUCTION

The deployment of subsurface energy sources is moving to gradually more complicated areas. Applications include geothermal operations in fractured reservoirs, shale gas production, but also more conventional gas production. As an example, studies into the origin of seismicity induced by gas production from the Groningen reservoir has resulted in complicated constitutive models that allow the distinction between elastic and plastic mechanical behavior. A whole gamut of complicated target areas enters the focus of engineers and scientists. Many challenges and issues are related to such complicated target areas: low permeabilities, induced seismicity, stabilities at deeper depths, economics, safety among others.[1,3–5] Engineers and scientists must be able to make realistic forecasts about these target areas to facilitate decision making. Example issues in decision making are borehole stability, reservoir stimulation, minimizing the induced seismicity.[6,7]

Scientific and engineering problems are usually approached by field studies, experimental laboratory investigations, and modelling. Modelling can be done though numerical, analytical, and semi-analytical investigations. All these approaches

are complementary, and their simultaneous development is important. Numerical investigations using finite elements, discrete elements, and finite differences (FDs) help to simulate the natural processes in a digital environment and scale laboratory results to the larger field. Analytical and semi analytical investigations help in understanding the physics of the actual problem, are computationally cheap and hence they are often employed for parameter searches and stochastic analyses, which usually require many models runs.[8] They can also be used validating numerical tools using on simulations before employing them to more complex scenarios. In this paper we present semi-analytical solutions.

The analytical solution for a circular opening in an infinite elastic medium was first given by Kirsch.[9] Later developments also considered plasticity models, like Mohr-Coulomb[10,11] and Hoek-Brown.[12,13] Details on the historical development can be found in Brown et al[14] and Singh.[15] Chen and Abousleiman,[16–18] and Singh et al[19–22] among others showed the way to implement a complex yield-surface-based model in semi-analytical and analytical schemes. Most of the uncoupled analytical and semi-analytical studies, however, focus only on the changes in stress and strain due to borehole construction under the condition of complete drainage.

An analytical formulation for the transient coupled behavior of rocks was proposed by Rice and Cleary,[23] within the extent of poro-elasticity. Detournay and Cheng[24] from their coupled poroelastic analysis around a pressurized well observed that failure can occur inside the rock rather than at the borehole opening. Bai and Roegiers[25] also included thermal coupling and observed the unexpected behavior of a pressure rebound. These fully coupled transient models, however, do not consider the inelastic or plastic behavior of the geomaterials. Therefore, some researchers adopted a steady-state flow equation in a poro-elastoplastic analysis. Such a treatment led Wang and Dusseault[26] to the conclusion that breakdown pressures cannot be estimated considering elasticity only. Han and Dusseault[27] calculated the change of porosity and permeability using a similar approach. Masoudian and Hashemi[28,29] studied adsorption-related phenomena like swelling and shrinkage. To address the gap between fully transient poroelastic models and steady-state poro-elastoplastic models, we[1] recently proposed a semi-analytical approach that takes care of the transient nature of the problem along with plasticity. The current paper extends the Mohr-Coulomb perfect plasticity model adopted earlier to a more realistic model.

The constitutive model adopted in this study was developed for the Slochteren sandstone found in the Groningen gas field, The Netherlands. Experiments on Slochteren sandstone revealed that the inelastic deformation contributes significantly in compressive deformation.[30–34] A plasticity model was proposed by Pijnenburg et al[33] to reflect this inelastic deformation. This model was derived from Cam-Clay plasticity model,[35] it was later modified by Singh et al[2] to a more general formulation. The implementation in our transient poro-elastoplastic model required a combination of numerical and analytical techniques, and the present paper shows how that was done. The solution considers porosity variations, permeability variations, elastic properties variations, and an evolution of the yield surface. Time stepping is a fundamental ingredient of our approach, and we show how rather complicated constitutive behavior in a transient setting can still be approached with a relatively fast semi-analytical approach.

In the following section, we briefly introduce the foundation of our current work: (a) the plasticity model proposed by Singh et al,[2] (b) the equations required to obtain the change in stresses and deformation after the construction of a borehole, and (c) the method adopted from Fokker et al[1] to calculate the pore-pressure change with time caused by injection or production. In the subsequent section, we present the methodology to calculate the change in stresses and deformation caused by these pressure changes for specific cases. We demonstrate the implementation with calculations for pure injection, shut-in, pure production, stimulation (involving a change the in situ permeability), and injection-production from a stimulated borehole. Finally, we close the article with a discussion of current issues and future scope of our method, and conclusions of the present study.

2 | MODEL DEVELOPMENT

2.1 | Plasticity model

Pijnenburg et al[33] modeled the mechanical response of Slochteren sandstone using an elliptical yield function similar to a modified Cam-Clay plasticity model. They needed this model, with an over-consolidation ratio R close to unity, because the mechanical response of the Slochteren sandstone under hydrostatic and deviatoric loading showed an inelastic deformation in all stages of compressive loading. In the current work we used a modified form of this model. The modifications include the introduction of a variable critical state slope M and non-linear elasticity. Both introductions were motivated by the experimental outcomes and the use of multiple values of M in Pijnenburg et al[33] plasticity model. The full motivation, description, and validation of our extension is provided in Singh et al.[2] That article further

discusses the Groningen reservoir's compaction and compares a borehole under drain state with the commonly used Mohr-Coulomb model. We here only provide the formulas required to support the description of the implementation of this model in our semi-analytic approach.

The yield surface of the plasticity model is defined as:

$$f\left(q, p', M, \sigma^*\right) = q^2 - M^2 p'\left(\sigma^* - p'\right) = 0 \tag{1}$$

where the deviatoric stress $q = \sqrt{\frac{1}{2}\left(\left(\sigma'_1 - \sigma'_2\right)^2 + \left(\sigma'_1 - \sigma'_3\right)^2 + \left(\sigma'_2 - \sigma'_3\right)^2\right)}$, the mean effective stress $p' = \frac{(\sigma'_1 + \sigma'_2 + \sigma'_3)}{3}$ with the effective stress defined according to Terzaghi ($\sigma'_i = \sigma_i - P$), and the parameter M is having a functional dependency on the inelastic volumetric strain. This is consistent with the experimental observations by Pijnenburg et al,[33] but it extends their analysis to a mathematically consistent one. The functional relationship of variable M is through an initial value and a slope which relates the change in M to the change in inelastic volumetric strain. This is analogous to the evolution of pre-consolidation pressure σ^* as in the original Pijnenburg et al[33] plasticity model. We thus have

$$M^t = M^{t-1} + \frac{\partial M}{\partial \epsilon^p_{p'}} d\epsilon^p_{p'} \tag{2a}$$

$$\sigma^{*t} = \sigma^{*t-1} + \frac{\partial \sigma^*}{\partial \epsilon^p_{p'}} d\epsilon^p_{p'} \tag{2b}$$

The elastoplastic stiffness matrix $\boldsymbol{S}$ for plastic loading relates total incremental strains $\Delta\epsilon$ to incremental stresses $\Delta\sigma$ (Singh et al[2]). Assuming the principal stresses and strains to align with the radial coordinate system, we have

$$\begin{bmatrix} \Delta\sigma'_r \\ \Delta\sigma'_\theta \\ \Delta\sigma'_z \end{bmatrix} = [\boldsymbol{S}] \times \begin{bmatrix} \Delta\epsilon_r \\ \Delta\epsilon_\theta \\ \Delta\epsilon_z \end{bmatrix} \tag{3}$$

where

$$[\boldsymbol{S}] = [\boldsymbol{C}]^{-1}$$

$$c_{ij} = H a^{'}_i \, a^{'}_j + \frac{1}{E}\left(-\nu + \delta_{ij}\left(1 + \nu\right)\right)$$

$$a^{'}_i = 3\left(\sigma'_i - p'\right) + \frac{p'}{3}\left(m^2 - \eta^2\right)$$

$$H = \frac{1}{\left(M^2 p' \frac{\partial \sigma^*}{\partial \epsilon^p_{p'}} + \frac{2q^2}{m}\frac{\partial M}{\partial \epsilon^p_{p'}}\right) \times p'\left(M^2 - \eta^2\right)}$$

$$\eta = q/p'$$

Here, E is the elastic Young's modulus, ν is Poisson's ratio, p' and q are the mean effective and the deviatoric stress, respectively.

We followed the approach of Hypo-elastic incremental formulation.[36] The variation of Poisson's ratio is defined by

$$\nu = k_o \left(\frac{\sigma_3}{p_a}\right)^{n_o} + \nu_o \tag{4}$$

An upper limit to the elastic modulus is defined with respect to minor principal stress magnitude:

$$E_{max} = k \times p_a \left(\frac{\sigma_3}{p_a}\right)^n + E_o \tag{5}$$

For $\sigma_3 = 0$, the limit value of the modulus is E_o. Triaxial test results[33] for Slochteren sandstone showed the non-linear behavior for the initial part of the deviatoric loading, this was incorporated in the constitutive model as

$$E/p_a = a_m + b_m\,(q/p_a) \quad \text{if } E \le E_{\max} \quad \text{and } \sigma_3 \le {\sigma_3}^{cri} \tag{6}$$

where

$$a_m = a_{m1} + a_{m2}\sigma_3/p_a$$

$$b_m = b_{m1} + b_{m2}\sigma_3/p_a$$

The equation relates the elastic modulus to the deviatoric stress, using two parameters a and b which have a functional dependency on the minor principal stress. $p_a = 1$ MPa is used to make the parameters in Equation (6) dimensionless. ${\sigma_3}^{cri}$ is a critical minor principal stress above which there is no effect due to the state of deviatoric stress on elastic modulus.

2.2 | Elasto-plastic stresses around the borehole

A borehole alters the subsurface state of stress through the inner stress boundary conditions at the borehole wall. The effect is concentrated around the opening; far away, the stresses are left largely unaffected. The present section summarizes the correlations describing the stress changes resulting from a borehole in a subsurface that is described by the new constitutive model; a full description can be found in Singh et al.[2]

The changes in stresses due to the presence of the borehole are given in terms of the auxiliary variable $\beta = \frac{u}{r_d} = \frac{r_d - r_o}{r_d}$ where u is the radial displacement, r_o is the original radial position, and r_d is the changed radial position. Using the auxiliary variable employs a Lagrangian formulation in which the development of volume elements is followed.[2,17,18,37–39] Once the relationship between the stresses and β has been established, the relation between the radial distance and β is used to calculate the stress as a function of position. The value of β for which the effective radial stress equals to borehole support pressure must correspond to the position at the borehole wall.

We have

$$\frac{D\sigma_r'}{D\beta} = \frac{\sigma_\theta' - \sigma_r'}{\left(1 - \beta - \left[\frac{e^{\epsilon_v}}{1-\beta}\right]\right)} \tag{7a}$$

$$\frac{D\epsilon_v}{D\beta} = \frac{\sigma_\theta' - \sigma_r'}{s_{11}\left(1 - \beta - \left[\frac{e^{\epsilon_v}}{1-\beta}\right]\right)} + \frac{(s_{12} - s_{11})}{s_{11}\,(1-\beta)} \tag{7b}$$

$$\frac{D\sigma_\theta'}{D\beta} = s_{21}\left\{\frac{\sigma_\theta' - \sigma_r'}{s_{11}\left(1 - \beta - \left[\frac{e^{\epsilon_v}}{1-\beta}\right]\right)} + \frac{(s_{12} - s_{11})}{s_{11}\,(1-\beta)}\right\} - \frac{(s_{22} - s_{21})}{(1-\beta)} \tag{7c}$$

$$\frac{D\sigma_z'}{D\beta} = s_{31}\left\{\frac{\sigma_\theta' - \sigma_r'}{s_{11}\left(1 - \beta - \left[\frac{e^{\epsilon_v}}{1-\beta}\right]\right)} + \frac{(s_{12} - s_{11})}{s_{11}\,(1-\beta)}\right\} - \frac{(s_{32} - s_{31})}{(1-\beta)} \tag{7d}$$

where σ'_r, σ'_θ, σ'_z are effective radial, tangential, out-of-plane stresses, respectively. ϵ_v is total volumetric strain.

The solution procedure starts with the initial condition calculated at the elastic-plastic interface - the boundary dividing the elastic and plastic zone. Then, Equations (7a-d) are employed for incrementally changing values of β to get the values of stresses and strains between the elastic-plastic interface and the inner boundary of the cavity.

In Pijnenburg et al's[33] plasticity model the elastic-plastic interface should lie at infinity. This is achieved by choosing R close to unity. Then all the stresses, the displacements, and the auxiliary variable β equal the values corresponding to the undisturbed, virgin stress state.

The volumetric plastic strain and the total volumetric strain at the interface are both zero, $\epsilon^p_{p'} = \epsilon_v = 0$. The value of β_o at the interface is approximated with constant values of the elastic parameters. This assumption will not cause significant errors, as the interface is very far from the well. β_o can be calculated under the assumption of linear elasticity:

$$\beta_o \sim \frac{\frac{(1+\nu)}{E}\left(\sigma'_r(\beta_o) - \sigma'_h\right)}{1 + \frac{(1+\nu)}{E}\left(\sigma'_r(\beta_o) - \sigma'_h\right)} \tag{8}$$

The relation between the radial distance r_d and auxiliary variable is given as:

$$\frac{r_d}{a} = e^{\int_{\beta(a)}^{\beta(r_d)} \frac{d\beta}{1-\beta-\frac{e^v}{1-\beta}}} \tag{9}$$

where $\beta(a)$ is the magnitude of the auxiliary variable at the inner boundary of the circular cavity, and a represents the deformed radius of the inner boundary. These results give the stresses and deformation in the reservoir at time equal to zero. Since R is close to unity this the entire rock mass is in the plastic domain, and the magnitude of the yield function (Equation [1]) is zero.

2.3 | Changes in pore fluid pressure due to operations

Many operations involve the injection and production of fluid. The resulting changes in the fluid pressure are input for the poro-elastoplastic stresses. We employ a semi-steady-state approach to approximate the solution to the pressure diffusion equation.[1] This approximation helps to formulate the pressure development also when permeability and porosity are changing over time.

For long enough times after rate changes, an approximate solution to the diffusion equation can be formulated with a logarithmic decay up to an influence radius.[1,40] Beyond the influence radius the change in the pore pressure is negligible. Inside it, the pressure is computed using Darcy's law under the assumption of negligible storage. The influence radius $r_e(t)$ is growing with time t according to the virgin diffusivity c. This is called the semi-steady-state approximation.

Darcy's law under the presumption of negligible storage within the pressure influence radius, with the injection rate defined as Q_{inj} (positive for injection) is given as a differential equation for steady-state flow:

$$\frac{d\Delta p}{dr} = -\frac{q(r)}{\lambda} = \frac{-Q_{inj}}{2\pi\lambda r h} \quad (\text{for } r < r_e\ (t)) \tag{10a}$$

In this equation $\lambda = k/\mu$ stands for the mobility, which is the ratio of permeability to viscosity. The solution is given by

$$\Delta P\ (r,t) = \int_r^{r_e(t)} \frac{Q_{inj}}{2\pi\lambda(\rho)\rho h} d\rho + \Delta P_{constant} \quad (\text{for } r < r_e(t)) \tag{10b}$$

$$r_e\ (t) = \sqrt{\frac{2.25 \cdot t}{c} + {a_o}^2} \tag{10c}$$

The influence radius (Eq. 10c) is a function of diffusivity and time. The diffusivity is

$$c = \frac{1}{\lambda}\left[\frac{1}{m} + \frac{\alpha^2}{2G}\cdot\frac{1-2\nu}{1-\nu}\right] \tag{11}$$

where $m = \frac{K_f}{\phi}\cdot\left[1+\frac{K_f}{\phi K_s}(1-\phi-\frac{K}{K_s})\right]^{-1}$ is the Biot modulus[41];

K_{fluid}, K_{solid}, and K are the bulk moduli of the fluid, the solid grains, and the rock, respectively; ϕ is the porosity; G is shear modulus, and α is Biot's coefficient given by $\alpha = 1-\frac{K_{fluid}}{K_{solid}}$. ϕ is updated with the change inelastic strains after every time increment. Note that the diffusivity c is used from the properties of the geomaterial at virgin in situ stress state. For the case of anisotropic material Biot's tensor is used.[42]

Injection is often applied for a finite time or injection rates are changing. Much the same as in usual well testing approaches, we employ superposition of solutions with different rates. As an example, in case of complete cessation of injection, solutions with opposite rates but different starting times are used.

The semi-steady-state approach facilitates the use of the actual mobility as a function of time and place. For multiple changes of rates at times t_i, the pressure at a certain time thus is a superposition of the contributions of all periods j with their own injection rates and radii of influence until that time:

$$\Delta P\ (r, t_n < t < t_{n+1}) = \sum_{j=1}^{n} \int_{\min\left(r, r_e^j(t)\right)}^{r_e^j(t)} \frac{{Q_{inj}}^j - \left({Q_{inj}}^{j-1}\right)}{2\pi\lambda\,(\rho)\,\rho h} d\rho \tag{12a}$$

$$r_e^j\ (t) = \sqrt{2.25\cdot\frac{t-t_{j-1}}{c} + {a_o}^2} \tag{12b}$$

For short times and quickly after changing rates, this approximation is not very good. This is related to the fact that the approximation was formulated for relatively large times. Results for such short timescales must thus be taken with care.

3 | CASE WISE IMPLEMENTATION

The coupled model discussed in the previous section has been implemented to solve the borehole mechanical behavior in various processes. We show how injection can cause stabilization after initial plasticity, how production can cause a continuation of plastic behavior, and how stimulation and injection and production cause complicated interference between plastic and elastic responses.

3.1 | Injection and shut-in (elastic loading and unloading)

Loading and unloading take place in an elastic way when a material experiences stresses below its yield limits, as defined by the yield surface. If, for example, a fluid is injected from a borehole into the reservoir around it, the stresses change due to the change in the in situ pore fluid pressure. For an elastic-perfectly plastic material, we already observed that injection thus causes the original plastic region to react elastically, until the stresses reach the tensile stress region.[1] In that study, we adopted the concept of criticality to describe this behavior. We defined criticality as the ratio of the actual and yield stress: it is below unity for the elastically reacting reservoir region and equal to unity in the plastically reacting region. The procedure was to first apply the equations for elastic loading and unloading; the results then were checked for the criticality. If needed, a plastic zone was defined, and the behavior of the complete domain was evaluated in an integrated way.

The concept of criticality is not used here. Instead, we use the magnitude of the yield function to define the state of the material. If the magnitude is below zero, it is in elastic state, and if it is above zero, it is in plastic state. If the magnitude of the yield function remains below zero, the material is concluded to react elastically.

The change of effective stress below the yield limit causes an elastic response, for which we adopt the concept of poro-elasticity.[43] The incremental effective stresses changes are related to the incremental strain in elastic regime as

$$\begin{bmatrix} \Delta\sigma_r' \\ \Delta\sigma_\theta' \\ \Delta\sigma_z' \end{bmatrix} = [\boldsymbol{B}] \times \begin{bmatrix} \Delta\epsilon_r \\ \Delta\epsilon_\theta \\ \Delta\epsilon_z \end{bmatrix} \tag{13}$$

where

$$b_{ij} = \frac{E}{1+\nu}\left(\frac{\nu}{1-2\nu} + \delta_{ij}\right)$$

The elastic parameters E and ν are state-dependent as explained in section 2.1. The incremental tangential, radial, and vertical strains in Equation (18) for plane-strain conditions are

$$\Delta\,\epsilon_r = \frac{d\delta u}{dr} \tag{14a}$$

$$\Delta\,\epsilon_\theta = \frac{\delta u}{r} \tag{14b}$$

$$\Delta\,\epsilon_z = 0 \tag{14c}$$

The axisymmetric equilibrium equation for the force balance after perturbations caused by injection is given in terms of effective stress:

$$\frac{d\Delta\sigma_r'}{dr} + \frac{\Delta\sigma_r' - \Delta\sigma_\theta'}{r} + \alpha\,\frac{d\Delta P}{dr} = 0 \tag{15}$$

Substitution of Equations (18) and Equation (19) in Equation (20) results in a differential equation for the radial deformation versus radial position:

$$\frac{d^2\delta u}{dr^2} + \frac{1}{r}\frac{d\delta u}{dr} - \frac{\delta u}{r^2} + \alpha\,\frac{d\Delta P}{b_{11}dr} = 0 \tag{16}$$

The general solution of this equation is given by

$$\delta u\,(r) = \frac{1}{r}\left[\int_{a_o}^{r}\left(r'\int_{r'}^{r_e}\alpha\frac{\partial\Delta P}{b_{11}\partial r''}dr''\right)dr'\right] + \frac{z_1 r}{2} + \frac{z_2}{r} = \frac{1}{r}\int_{a_o}^{r} r' I_P\left(r'\right)dr' + \frac{z_1 r}{2} + \frac{z_2}{r}$$

$$I_P\,\left(r'\right) = \int_{r'}^{r_e}\frac{\alpha}{b_{11}}\frac{\partial\Delta P}{\partial r''}\,dr'' \tag{17}$$

and substitution of this result in Equations (19) and (18) yields

$$\Delta\,\epsilon_r = -\frac{1}{r^2}\int_{a_o}^{r} r' I_P\left(r'\right)dr' + I_P\left(r\right) + \frac{z_1}{2} - \frac{z_2}{r^2}$$

$$\Delta\,\epsilon_\theta = \frac{1}{r^2}\int_{a_o}^{r} r' I_P\left(r'\right)dr' + \frac{z_1}{2} + \frac{z_2}{r^2}$$

TABLE 1 Parameters used for representing the mechanical behavior of Slochteren sandstone of porosity 26.4% at temperature 100°C, as per section 2.1, stress-deformation analysis of a borehole as per section 2.2 and pore-pressure distribution from section 2.3

Parameter	Value	Parameter	Value	Parameter	Value	Parameter	Value
m_o	1.75	k_o	0	Depth	2500 m	K_{solid}	41 GPa
$\frac{\partial m}{\partial \epsilon^p_{p'}}$	−7	n_o	0	h	100 m	σ'_h	30 MPa
$\frac{\partial \sigma^*}{\partial \epsilon^p_{p'}}$	9708 MPa	ν_o	0.23	k_p (Permeability)	20 md	σ'_v	50 MPa
k	2000	a_m	140. σ'_3/p_a + 600	μ (viscocity)	0.29 mPa.s	P_w (Borehole Support Pressure)	0
n	0.43	b_m	30. σ'_3/p_a + 100	T	100 °C	Radius, a_o	0.1 m
E_o	2000 MPa	${\sigma_3}^{cri}$	50 MPa	K_{fluid}	2 GPa		

$$\Delta\sigma'_r = \frac{E}{(1+\nu)(1-2\nu)}\left\{(2\nu-1)\frac{1}{r^2}\left(\left[\int_{a_o}^{r}(rI_P(r))\,dr\right]-z_2\right)-(\nu-1)I_P(r)+\frac{z_1}{2}\right\}$$

$$\Delta\sigma'_\theta = \frac{E}{(1+\nu)(1-2\nu)}\left\{(2\nu-1)\frac{1}{r^2}\left(\left[\int_{a_o}^{r}(-rI_P(r))\,dr\right]-z_2\right)+\nu I_P(r)+\frac{z_1}{2}\right\}$$

$$\Delta\sigma'_z = \frac{\nu E}{(1+\nu)(1-2\nu)}\{z_1+I_P(r)\} \tag{18}$$

The two constants in the solution must be evaluated using two boundary conditions. The first condition is that δu must be zero for the radial distance r approaching infinity. Hence, $z_1 = 0$. The second condition is that at the opening of the borehole the change in effective radial stress must be zero:

$\sigma'_r = 0$ at $r = a_o$. The value of constant z_2 then is determined as

$$z_2 = {a_o}^2\left[\frac{(1-\nu)I_P(a_o)}{(2\nu-1)}\right] \tag{19}$$

We consider the sign convention that compressive normal stresses and strains be positive the following relationships between induced total stress $\Delta\sigma_{ij}$, strain ε_{ij}, and pore pressure increase ΔP.

$$\Delta\sigma_{ij} = 2G\left[\varepsilon_{ij}+\frac{\nu}{1-2\nu}\varepsilon\delta_{ij}\right]+\alpha\Delta P\delta_{ij} \tag{20}$$

The elastic solution facilitates the calculation of the yield function. For values below 0, the mechanical response is indeed elastic; for values above 0 the alternative plastic behavior must be applied.

An important note must here be made in relationship to the parameters M and σ^*: for elastic unloading and reloading they are fixed. This is related to the definition of the evolution for these parameters, being a function of inelastic/plastic volumetric strains only.

The current equations can be used for injection, shut-in and even for injection and production cases if the process is within the elastic regime. We take as an example a simple injection case with material parameters for the Groningen sandstone.[2]

For the in situ stresses and borehole dimensions, we also take values typical for the Groningen field conditions. The input is provided in Table 1. The over-consolidation ration R is taken $1+10^{-10}$, very close to the unity.

We first calculated the response of the borehole before any pore pressure disturbance, using the approach outlined in section 2.2. The outcome represents the stresses and deformations at time zero. At this stage there is no development of the excess pore-pressure, and the solution is formulated for a complete drainage condition.[2]

The injection of fluid causes the pore pressure to rise. The change in pore fluid pressure is calculated using the equations provided in section 2.3. Input parameters relevant for flow are also listed in Table 1. The development of the pressures, for an injection rate of $Q_{inj} = 0.6$ m^3/min, is presented in Figure 1A. A logarithmically decreasing pressure propagates into

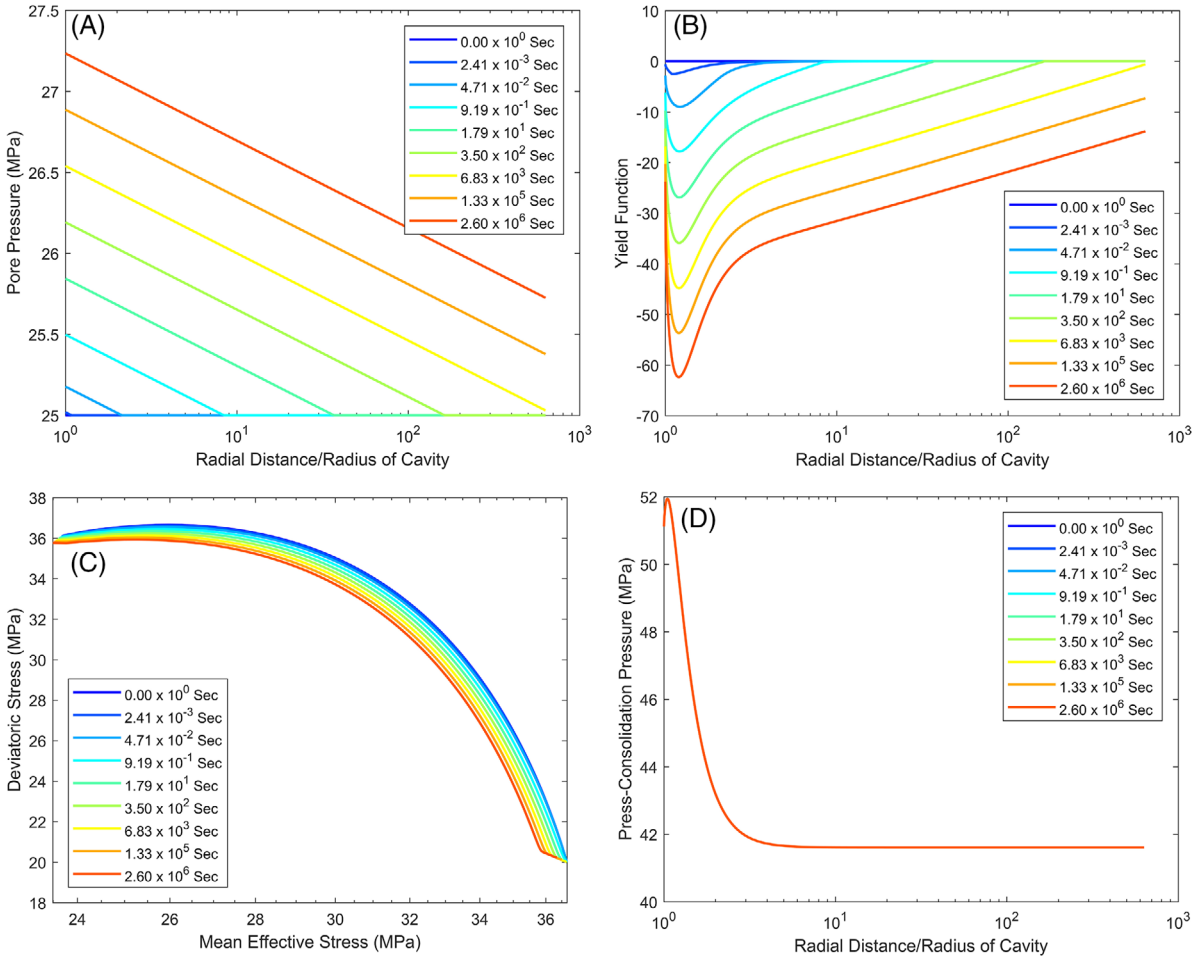

FIGURE 1 The effect of injection (A) change in in situ pore-pressure with time (B) check for the yield state of geomaterial (C) stress curves for successive time increment (D) inelastic strains

the reservoir, while the influence radius of the pressure is increasing. As a result, the pressure at the wellbore increases with time.

Now we proceed to calculating the influence of changing pore pressure. At every time step the pore-pressure increase is input for Equations (22) and (23). The new stress state is checked for the state of yielding using Equation (1): if the yield function is less than zero the material reacts elastically; else it reacts plastically. We observe that, in this case of injection, the stresses are in elastic region (Figure 1B). Stress curves (Figure 1C) drawn for these time steps also show successive curves lies just below the previous ones. This also indicates that the injection process causes elastic unloading.

The effective stresses and deformations are shown in Figure 2. Figures 2A-2C show that the magnitude of all effective stresses is continuously reducing. This is due to the increase in pore pressure. An interesting observation is the deformation shown in Figure 2D: larger deformations occur far from the borehole, and they are directed outward, away from the wellbore.

In the current constitutive model, the critical state slope and the elastic modulus are variables. They depend on the volumetric inelastic strains and stresses; hence the current solution takes into account a change in modulus and various associated properties such as Biot's coefficient. Figures 3A-3D show the variation of the critical state slope M, pre-consolidation pressure, elastic modulus, and Biot coefficient. The critical state slope decreases, and pre-consolidation pressure increases near the borehole, which suggests that the material shows dilation in this region. No temporal variation of the critical state slope and pre-consolidation pressure is observed, because they are functionally related to the inelastic volumetric strain as observed by Figure 1D. On the contrast, the injection process alters the stresses; as a result, the elastic properties show some variation (Figure 3C). On their turn, these variations cause changes in the Biot's coefficient. The rock mass reacts elastically because, while all effective stresses are reduced, the largest one (the tangential stress) is reduced most. Faults

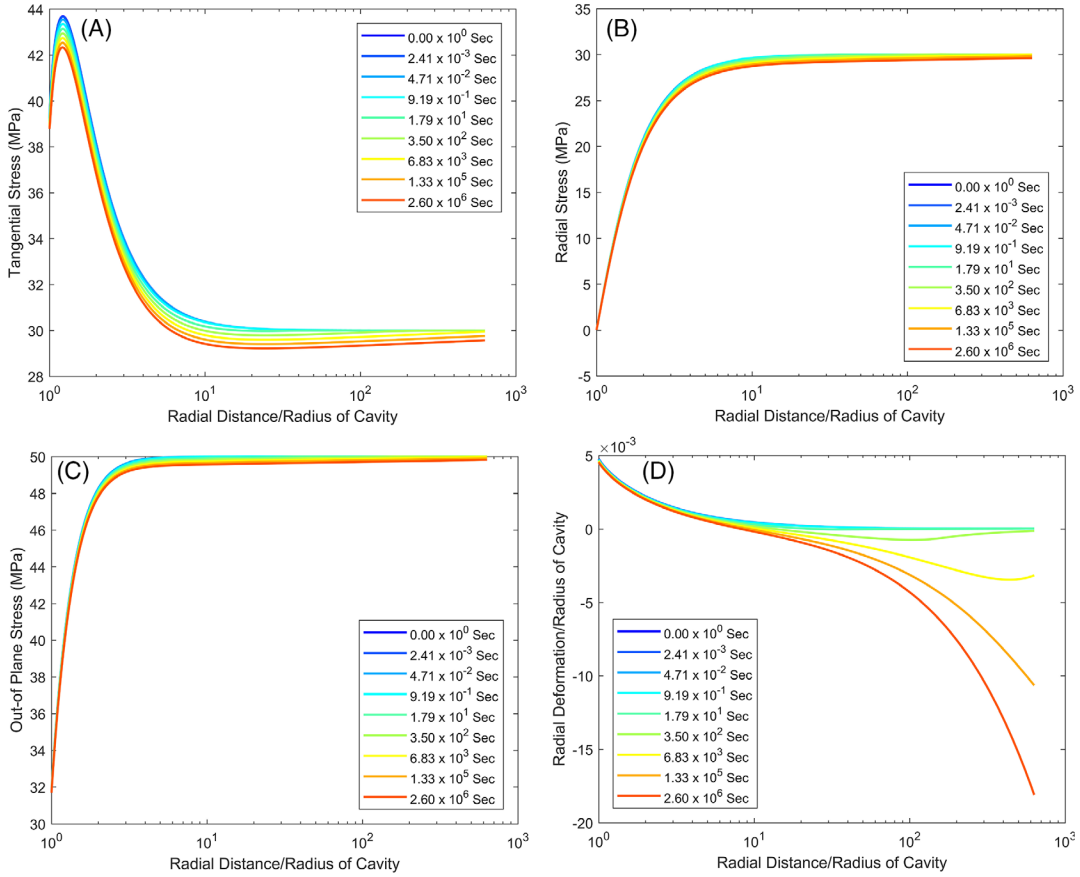

FIGURE 2 The effect of injection: Spatial and temporal variation of stresses (A) tangential (B) radial (C) out-of-plane stresses respectively and (D) radial deformation

near the borehole will be stabilized - but we note that calculations were performed under isothermal conditions and under the assumption of isotropic virgin stresses.

We also simulated well shut-in following the first injection for 2.6×10^6 seconds with $Q_{inj} = 0.6$ m^3/min. The superposition approach from section 2.3 was employed. The calculated pore-pressure and the associated magnitudes of the yield function are represented in Figure 4. The process is elastic because the magnitude of yield function is negative: pore pressures do not drop below the in situ pore-pressure.

We observed earlier[1] that for shorter timescales the results from the superposition do not agree with the FD results. This is related to the approximation that is used for the pressure solution: it is less precise for short times after a change of rate. Results before 2.6×10^2 seconds after such a rate change should be considered with caution.

The changes in stresses and deformation are shown in Figures 5A-5D. During shut-in the material is reloaded, and the stresses return to the stresses immediately after construction.

3.2 | Production (plastic loading)

Loading a material while it is already at the yield surface can result in a plastic response. This can originate from production from a borehole, which causes a pore fluid pressure drop below the virgin pore pressure and an associated rise of the effective stresses. Plastic loading was also observed by Fokker et al[1] for production from a well in an elastic-perfectly plastic material.

We want to calculate the stresses and deformations due to plastic loading. To this end we insert the definition of incremental strains defined by the Equations (19a-c) in the plastic constitutive equation (Eq. 3), and substitute the result in

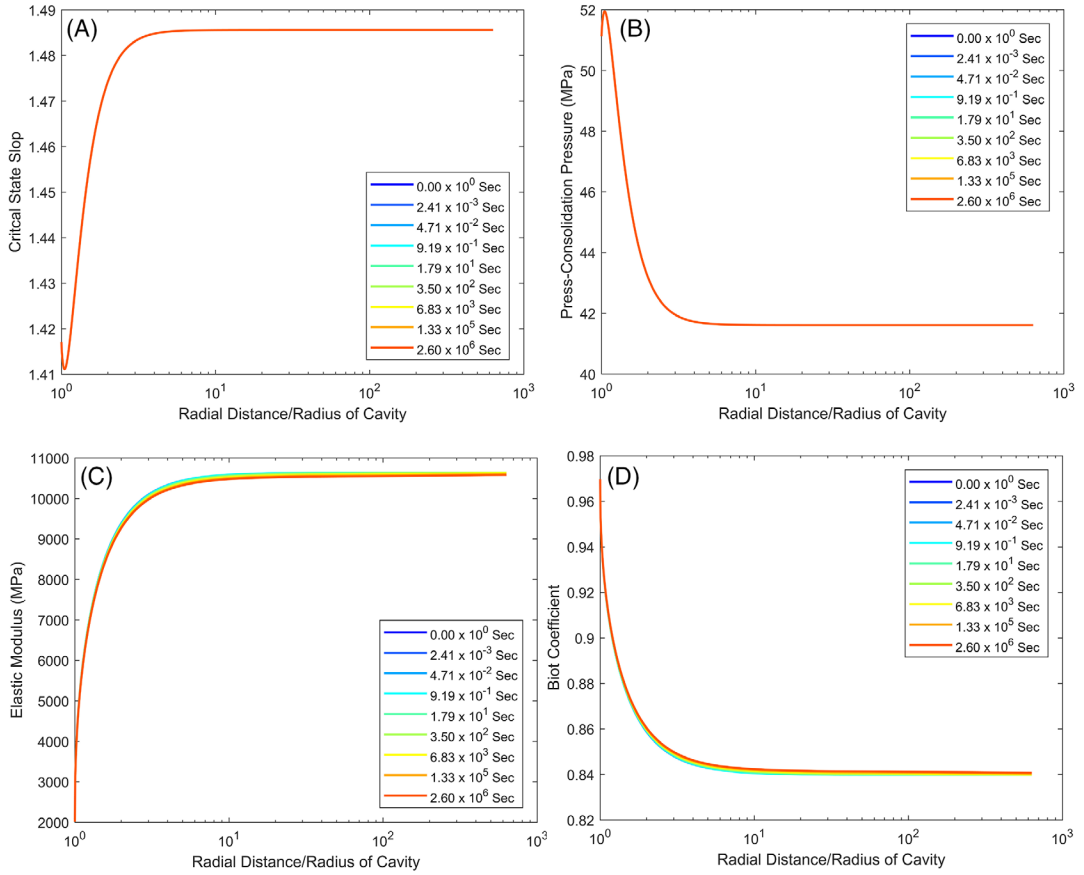

FIGURE 3 The effect of injection: spatial and temporal variation of (A) crtical state slope (B) pre-consolidation pressure (C) Young's modulus (D) biot coefficient

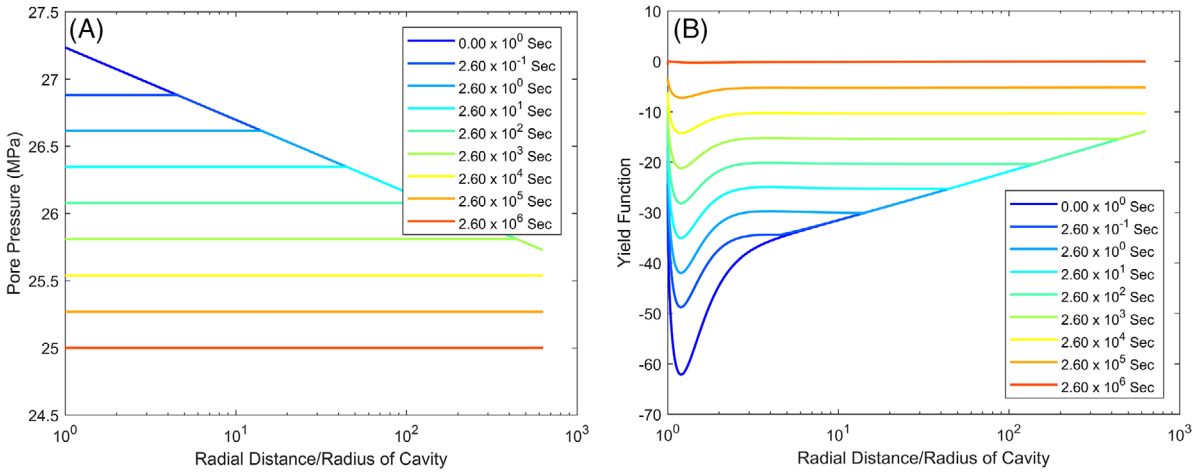

FIGURE 4 The effect of shut-in (A) change in in situ pore-pressure with time (B) check for the yield state of geomaterial for successive time increment

the equilibrium equation (Eq. 20). The incremental radial deformation and position then is governed by a second order differential equation:

$$\frac{d^2\delta u}{dr^2} + \frac{1}{r}\frac{d\delta u}{dr} - \frac{s_{22}\delta u}{s_{11}r^2} + \alpha\frac{d\Delta P}{s_{11}dr} = 0 \tag{21}$$

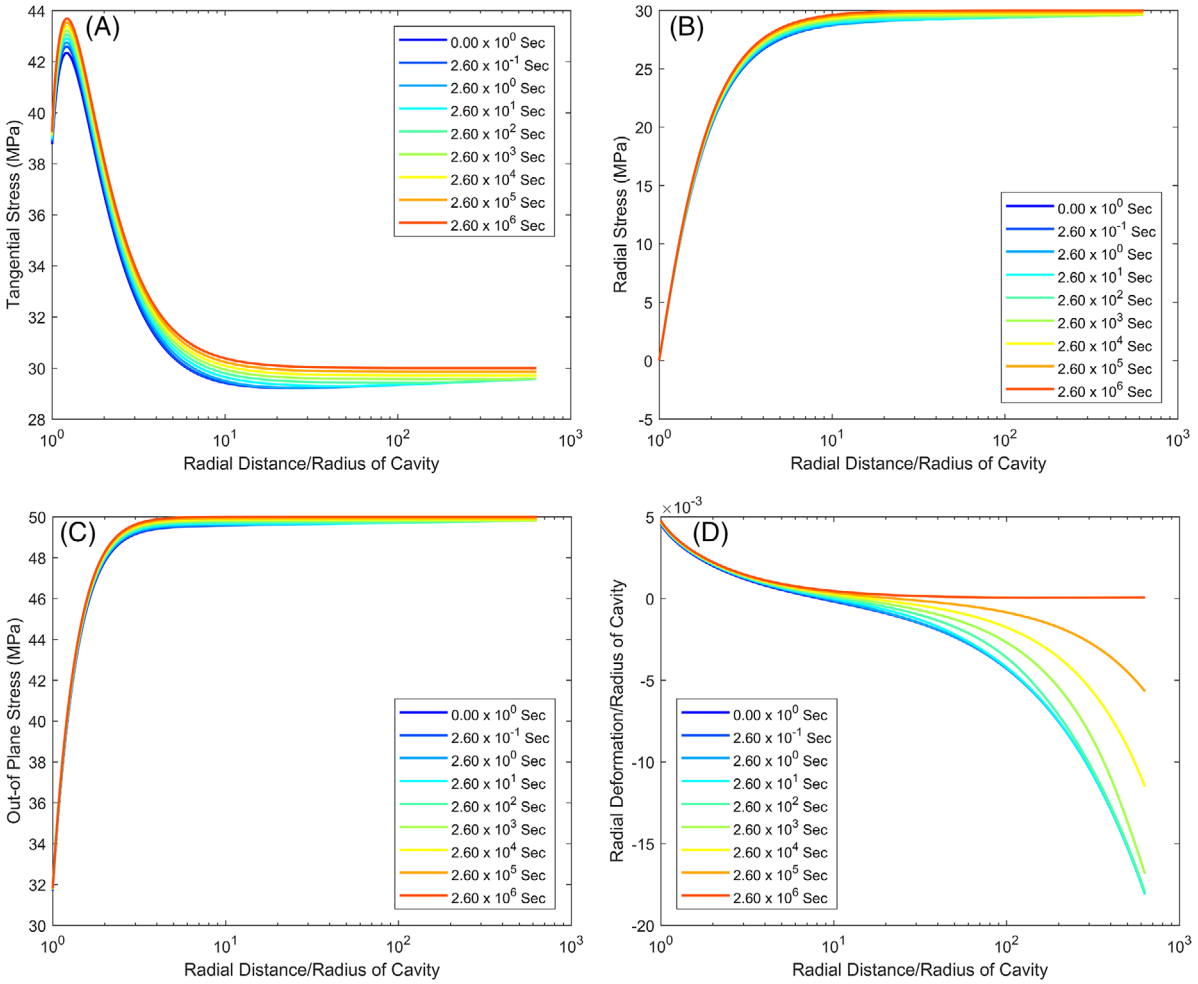

FIGURE 5 The effect of shut-in: spatial and temporal variation of stresses (A) tangential (B) radial (C) out-of-plane stresses respectively and (D) radial deformation

This equation is similar to the corresponding equation for the elastic response (Eq. 20) but differs in the coefficient of the term $\frac{\delta u}{r^2}$ is $\frac{s_{22}}{s_{11}}$, which was unity in Equation (20). This coefficient depends on the volumetric strain and thus on the displacement itself. We therefore solved it numerically using a numerical boundary value problem solution technique: the *bvp5c* solver in MATLAB.[44]

The boundary conditions for the production case are the same as for injection (see the previous section): zero incremental radial deformation far from the borehole, and zero incremental effective radial stress at the borehole opening. We have accepted a slight mismatch with the first condition by choosing a finite maximum distance from the borehole. The error can be minimized by choosing the boundary far enough from the borehole.

The numerical solution to Equation (26) and its boundary conditions provides incremental displacements and incremental radial strains in space and time. The incremental displacements are used to calculate incremental tangential strains, and, finally, Equation (3) is deployed to calculate the incremental stresses.

We here need to make a note related to the parameters M and σ^*: their values evolve in space and time during plastic loading. This is related to the constitutive model prescribing them: the parameters are functions of the inelastic/plastic volumetric strains that develop due to the plastic loading.

Let us turn to an example, with properties from Table 1. We first estimated an assumed elastic response using the equations of section 3.1. As the resulting elastic loading would load the material beyond its yield limit, the approach presented in the present section was adopted. The results from the analysis are shown in Figures 6, 7, and 8.

Figure 6A shows the change in the pore-pressure due to production. Production causes depletion of the fluid pressure, an increase of effective stress and plastic loading of the material. The yield function is very close to zero (order 10^{-11}),

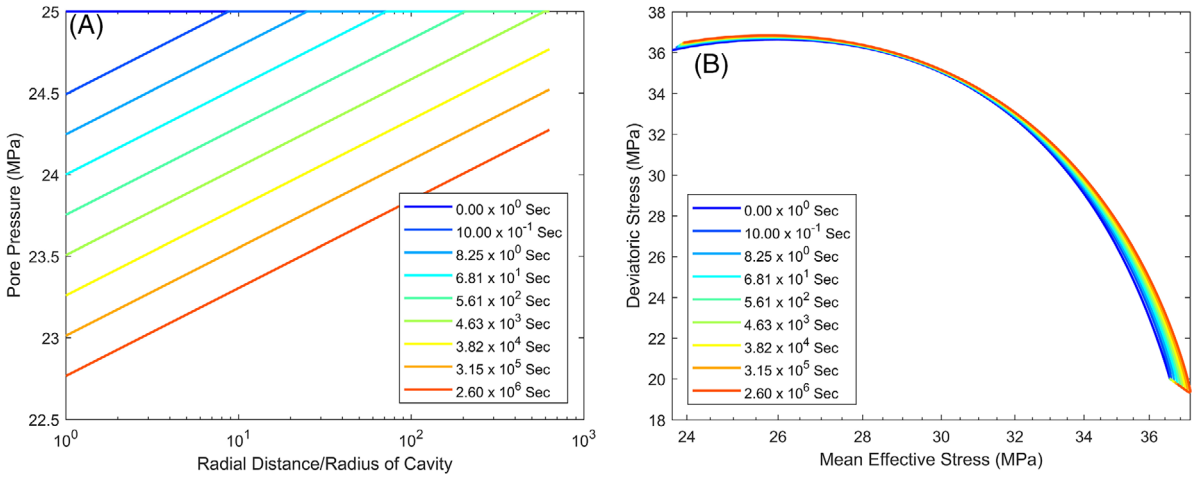

FIGURE 6 The effect of production (A) change in in situ pore-pressure with time (B) stress curve for successive time increment

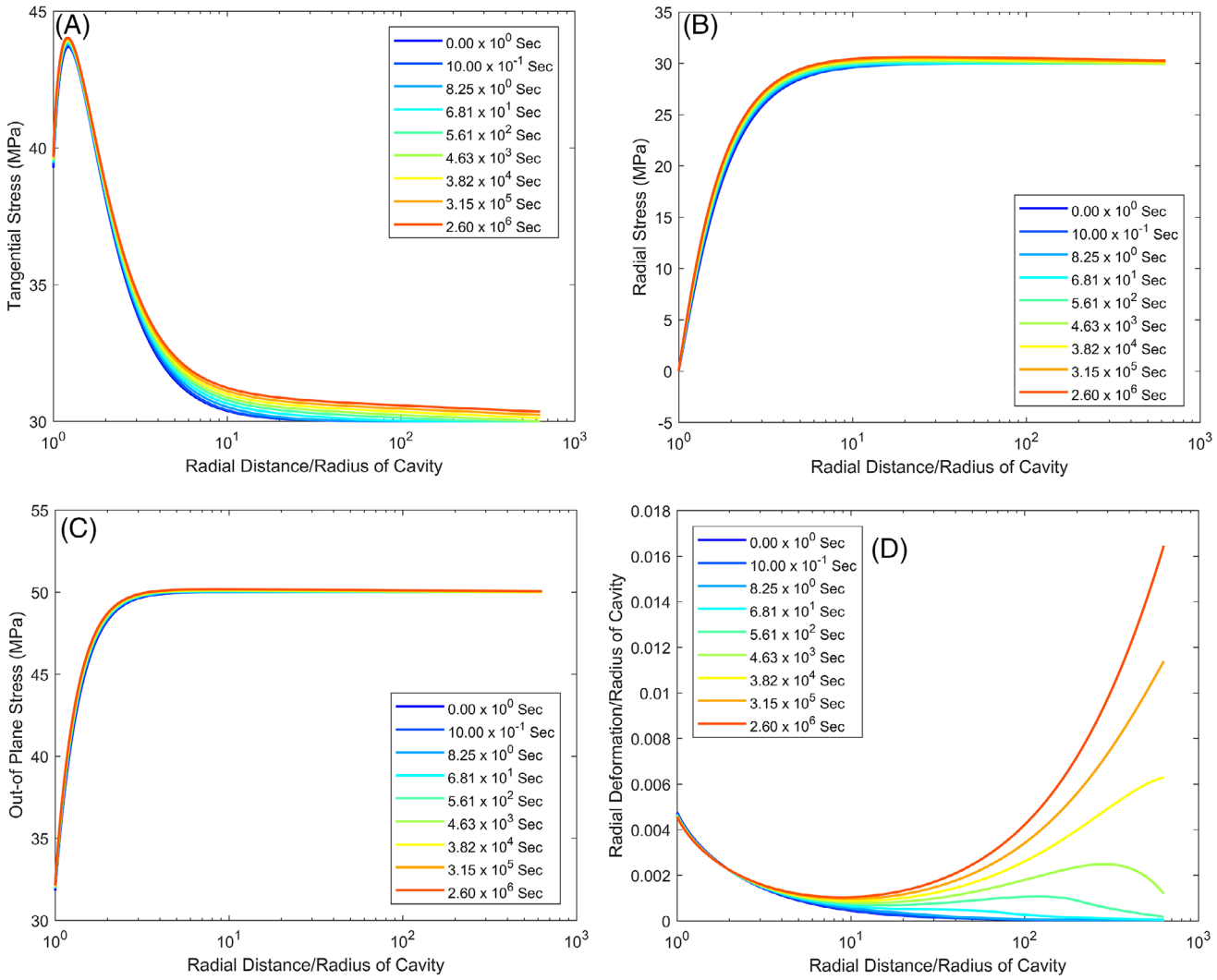

FIGURE 7 The effect of production: spatial and temporal variation of stresses (A) tangential (B) radial (C) out-of-plane stresses respectively and (D) radial deformation

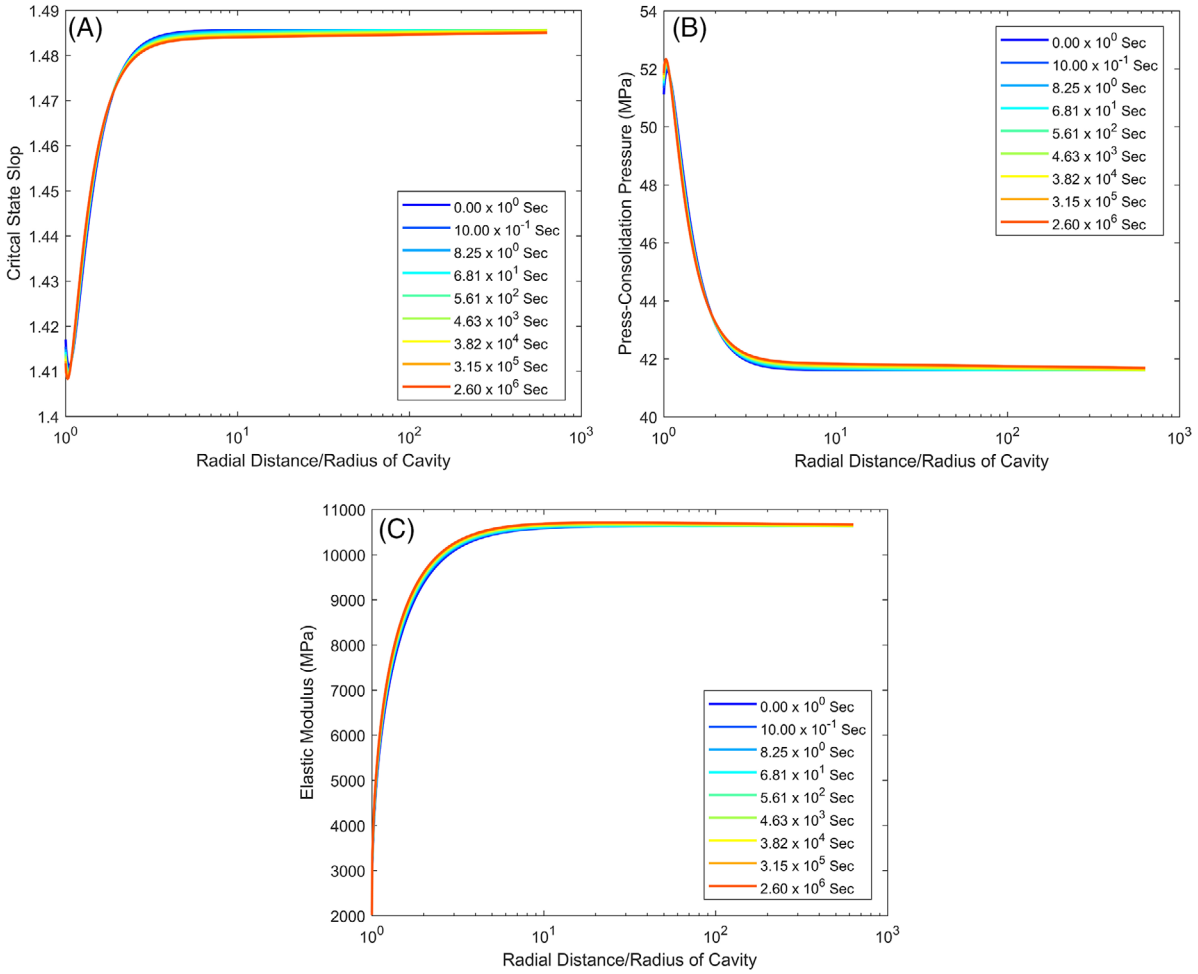

FIGURE 8 The effect of production: spatial and temporal variation of (A) crtical state slope (B) pre-consolidation pressure (C) Young's modulus (D) biot coefficient

indicating that the stresses are on the yield surface. Figure 6B shows the stress curve of the successive time steps. The yield surface size increases to accommodate the excess load.

The effective stresses and deformations for selected time steps are shown in Figure 7. The effective stresses increase in all principal directions. Increasing effective stresses result in increasing elastic modulus values. This can be observed from the Figure 8C, and we observe in Figure 7D the associated decreasing deformation at the borehole with successive time steps. Since the material is hardening, we observe a rise in stresses close to the borehole - for a softening material production could lead to an effective-stress drop.

Production causes plastic loading and inelastic deformation at every successive time step. The inelastic strains cause a change in the critical state slope and pre-consolidation pressures, as reflected in Figures 8A and 8B. The variation of the elastic modulus and Biot's coefficient also are represented in Figures 8C and 8D. Near the borehole, Biot's coefficient is close to unity; far away it is close to 0.84. The formulation that we have followed incorporates the variability of the important parameters.

3.3 | Stimulation

We also wish to incorporate the effect of injection or production on the reservoir permeability. The permeability modification affects the pore pressure distribution around the borehole through the functional dependency shown in section 2.3.

We follow our earlier approach,[1] which was based on the work by Bai and Elsworth.[45] It assumes that the effective permeability is determined completely by the fracture network. They related the permeability through a cubic function,

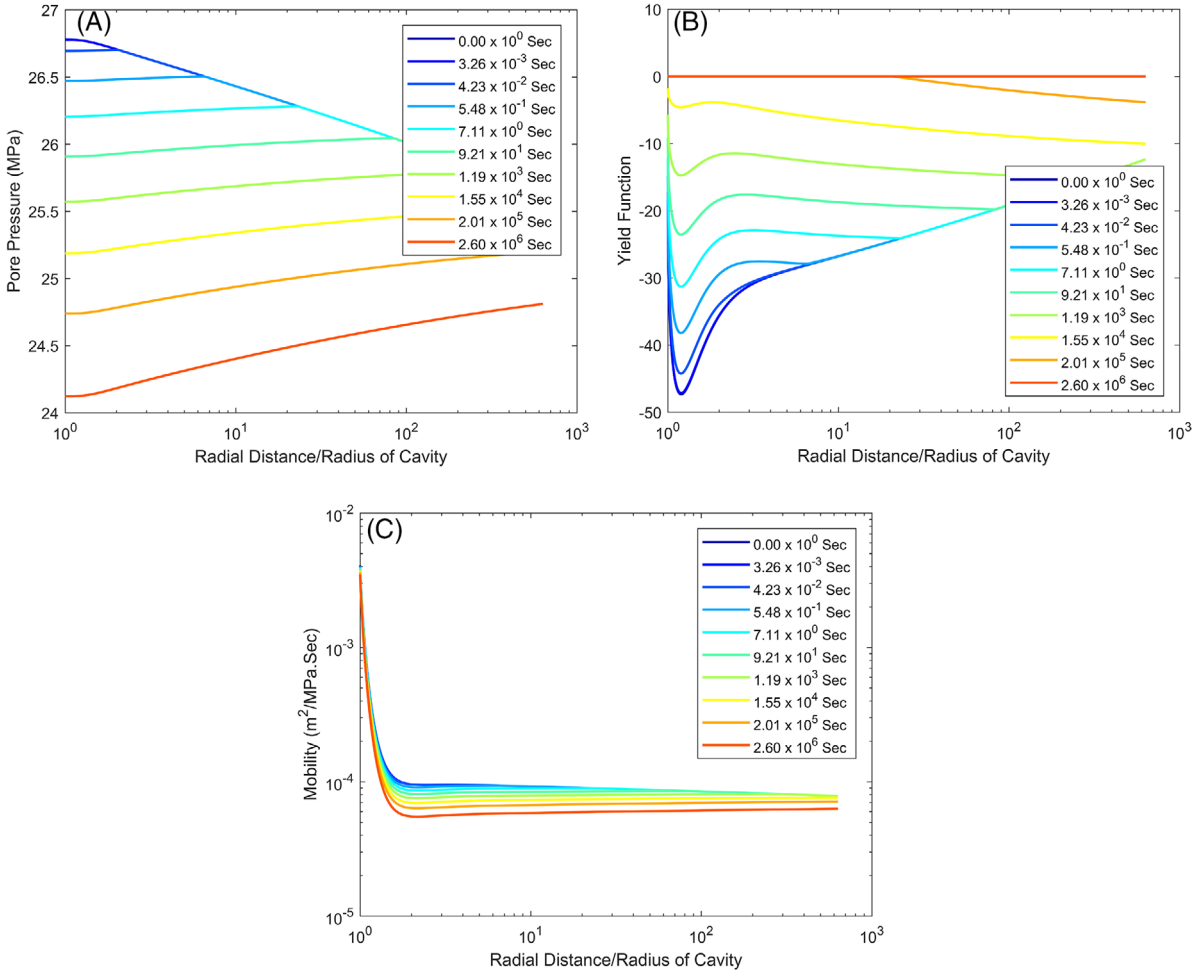

FIGURE 9 Demonstration of production after injection and stimulation (A) change in in situ pore-pressure with time (B) check for the yield state of geomaterial (C) mobility for successive time increment

given as:

$$k = k_0\left(1 - \frac{s\Delta\varepsilon}{b_0}\right)^3 = k_0\left(1 - \frac{s\Delta\varepsilon}{\sqrt[3]{12k_0 s}}\right)^3 = k_0\left(1 - \sqrt[3]{\frac{s^2}{12k_0}}\Delta\varepsilon\right)^3 \tag{22}$$

Where, k_0 is the virgin in situ permeability, s is the joint spacing, and $\Delta\varepsilon$ the average of radial and tangential strains (positive for compressive). The permeability increases with dilatational strain $\Delta\varepsilon$; larger joint spacings s have a larger effect in this nonlinear relationship. The permeability update is performed on every successful time step; updated values are used for every consecutive pore-pressure update. On their turn, these pore-pressure updates affect the incremental effective stresses and strain magnitudes.

To show the effect of permeability change, we devised an example, considering the same inputs as for the injection case (section 3.1). A value of joint spacing s of 0.05 m was employed. The result of the pore-pressure development in injection with stimulation is shown in Figure 9A at time t equal to zero. Its character of small-time steps in the analyses. Small discontinuities are resolved in the next timestep when the domains of elastic and plastic responses are reevaluated.

We accompany this last case also by an example - injection and production from the same borehole. The injection rate is taken the same as in the previous cases discussed. After performing injection at 0.6 m^3/min for 2.6×10^6 seconds (30 days), the fluid is produced from the borehole at a rate of −0.06 m^3/min. The production causes depletion of the pore pressure (Figure 9A). Whether the process is elastic or plastic is determined from the sign of the yield function (Figure 9B). The

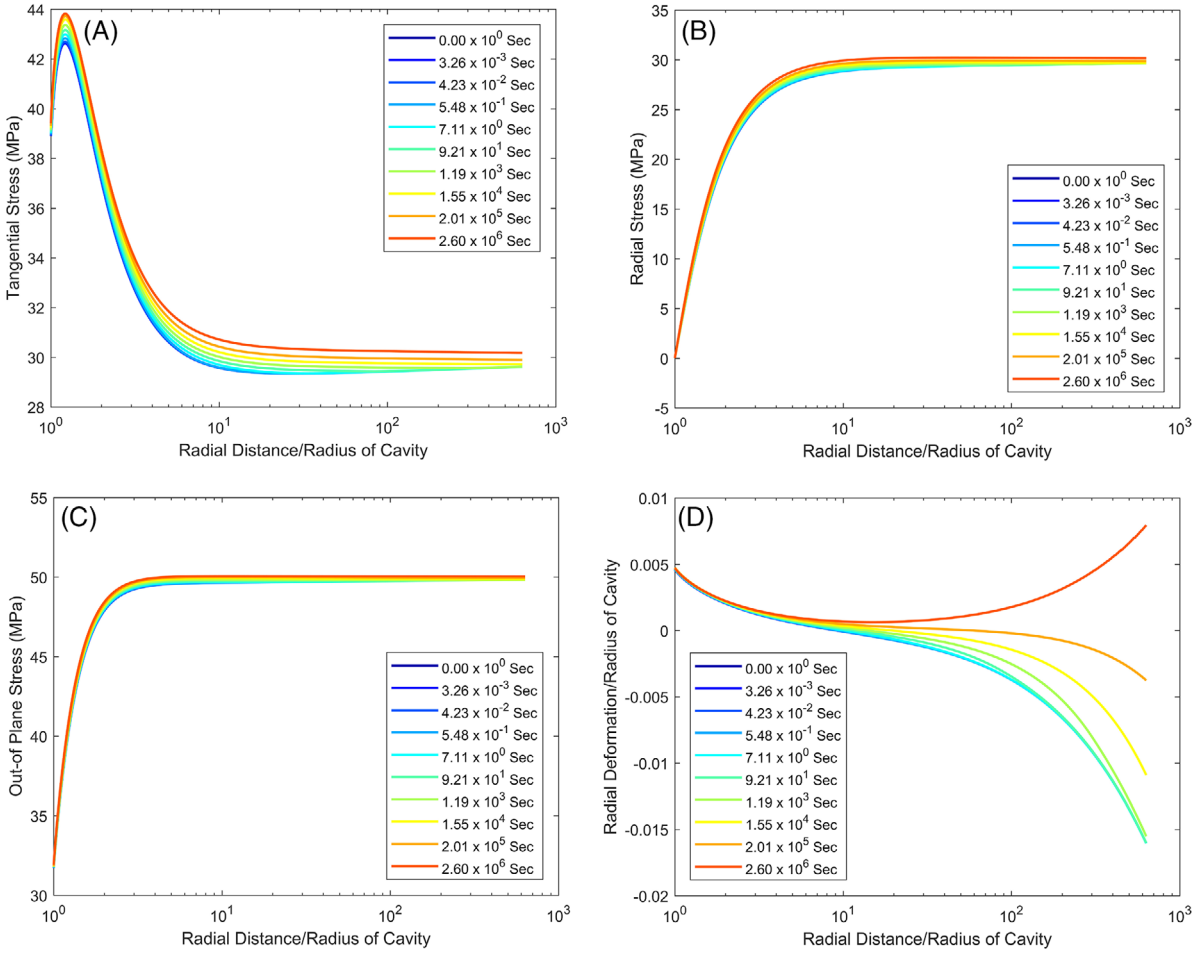

FIGURE 10 Demonstration of production after injection and stimulation: spatial and temporal variation of stresses (A) tangential (B) radial (C) out-of-plane stresses respectively (D) radial deformation

mobility, presented in Figure 9C, decreases with time as the production takes place: the fracture closes due to depletion of pore-pressures, which is similar to the trend observed for the elastic-perfectly plastic model.[1]

Figure 10 presents the effect of injection and production on stresses and deformation. The pressure drop resulting from the production results in an increase of the effective stresses (Figures 10A-10C). The outward deformation that was induced by the injection is reversed by the subsequent production.

4 | DISCUSSION

Different geological material reacts differently on loading, and simple generalized descriptions are not always adequate for calculating the mechanical response. Pijnenburg et al[33] and Singh et al[2] showed that the unique inelastic behavior of Slochteren sandstone requires unconventional constitutive laws to predict the compaction behavior of the Groningen reservoir. In this work, we have successfully demonstrated that such a complex constitutive model can be implemented in a fast-semi-analytical transient approach as the one we proposed earlier.[1]

The solution proposed in the current work is limited to axisymmetric loading. For some generalized constitutive laws, semi-analytic non-axisymmetric solutions have been developed for non-hydrostatic conditions.[37,46,47] These approaches, however, are far too complicated to use in the current context of complex constitutive behavior. Therefore, there is an urgent need to develop a simplified model handling the horizontal stress anisotropy.

The current model has been formulated for isothermal conditions. The incorporation of temperature poses two challenges. Firstly, the inclusion of temperature diffusion and convection in the model. These effects, however, have already been studied broadly,[48] and we could start implementing existing approaches. The second challenge is the effect of

cooling on the rock itself, which has been observed experimentally to be an important effect (see, e.g.[49–51] among others). Researchers as Parisio et al[52] describe a temperature-dependent yield surface to accommodate the temperature response. The use of such a yield surface could address the time-independent behavior of rock, but temperature also affects the time-dependent behavior.[53] The implementation of a robust temperature scheme would thus be one of the challenges. The limitations of the current model are that it is rate-independent, isotropic, and isothermal. Models for rocks that circumvent these limitations[54–56] can be considered for future work.

5 | CONCLUSIONS

In this study an advanced constitutive law has been implemented in the semi-analytical approach that had been proposed earlier.[1] The implementation accounts for the transient development of pressures and can handle multiple injection and production phases. The constitutive model had been developed for the Slochteren sandstone found in the Groningen gas field, The Netherlands, for which experiments had revealed the significance of inelastic deformation in compression.[33] The transient solution proposed in this article employs both numerical and analytical elements, and incorporates porosity variations, permeability variations, elastic properties variation, and the evolution of yield surface with time. A suite of cases, like injection, shut-in, production, stimulation, and injection-production, are discussed in the article. In this way we demonstrate the applicability of the proposed solution in various engineering problems. The application to geothermal energy applications calls for substantial improvements, the two most important ones being thermal effects and the effect of horizontal stress anisotropy.

ACKNOWLEDGMENTS

The project leading to the results in this article received funding from the European Union's Horizon 2020 research and innovation programmes under grant agreement number 691728 and under grant agreement number 727550.

ORCID

Peter A. Fokker https://orcid.org/0000-0001-9366-1497

REFERENCES

1. Fokker PA, Singh A, Wassing BB. A semianalytic time-resolved poro-elasto-plastic model for wellbore stability and stimulation. *Int J Numer Anal Methods Geomech*. 2020;44(7):1032-1052.
2. Singh A, Fokker PA, Pijnenburg RPJ, Spiers CJ. A formalized elasto-plastic constitutive model for a high-porosity reservoir sandstone and application to borehole stability analysis. 2020. (In press)
3. Wassing BBT, Van Wees JD, Fokker PA. Coupled continuum modeling of fracture reactivation and induced seismicity during enhanced geothermal operations. *Geothermics*. 2014;52:153-164.
4. Lu SM. A global review of enhanced geothermal system (EGS). *Renewable Sustainable Energy Rev*. 2018;81:2902-2921.
5. Lee KK, Ellsworth WL, Giardini D, et al. Managing injection-induced seismic risks. *Science*. 2019;364(6442):730-732.
6. Ghassemi A. A review of some rock mechanics issues in geothermal reservoir development. *Geotech Geol Eng*. 2012;30(3):647-664.
7. Hofmann H, Zimmermann G, Farkas M, et al. First field application of cyclic soft stimulation at the Pohang Enhanced Geothermal System site in Korea. *Geophys J Int*. 2019;217(2):926-949.
8. Jansen JD, Douma SD, Brouwer DR, Van Den Hof PMJ, Bosgra OH, Heemink AW.. Closed-loop reservoir management. Paper presented at SPE Reservoir Simulation Symposium 2009. The Woodlands, TX; United States; 2 February 2009 through 4 February 2009.
9. Kirsch G. Die theorie der elastizitat und die bedurfnisse derfestigkeitslehre. *Zeitschrift der Vereins deutscher Ingenieure*. 1898;42:797-807.
10. Mohr O. Welche Umsta ïde bedingen die Elastizitätsgrenze undden Bruch eines Materials? *Zeit des Ver Deut Ing*. 1900;44:1524-1530.
11. Coulomb CA. Sur une application des regles maximis et minimis aquelques problems de statique, relatives a l'architecture. *Acad Sci Paris Mem Math Phys*. 1776;7:343-382.
12. Hoek E, Brown BT. Empirical strength criterion for rock masses. *J Geotech Eng Div, ASCE*. 1980;106(GT9):1013-1035.
13. Hoek E, Carranza-Torres C, Corkum B. Hoek-Brown failure criterion 2002 edition. Paper presented at: Proceedings of NARMS-TAC; 2002; Toronto, Canada.
14. Brown ET, Bray JW, Ladanyi B, Hoek E. Ground response curves for rock tunnels. *J Geotech Eng*. 1983;109(1):15-39.
15. Singh A. *Closed-Form Solutions for Circular Cavity in Brittle and Ductile Rocks Using True Triaxial Strength Criteria under Plane Strain*. New Delhi: Indian Institute of Technology Delhi; 2018.
16. Chen SL, Abousleiman YN. Exact undrained elasto-plastic solution for cylindrical cavity expansion in modified Cam Clay soil. *Géotechnique*. 2012;62(5):447-456.

17. Chen SL, Abousleiman YN. Exact drained elasto-plastic solution for cylindrical cavity expansion in modified Cam Clay soil. *Géotechnique*. 2013;63(6):510-517.
18. Chen SL, Abousleiman YN. Wellbore stability analysis using strain hardening and/or softening plasticity models. *Int J Rock Mech Min Sci*. 2017;93:260-268.
19. Singh A, Rao KS, Ayothiraman R. Effect of intermediate principal stress on cylindrical tunnel in an elasto-plastic rock mass. *Procedia Eng*. 2017;173:1056-1063.
20. Singh A, Kumar C, Kannan LG, Rao KS, Ayothiraman R. Engineering properties of rock salt and simplified closed-form deformation solution for circular opening in rock salt under the true triaxial stress state. *Eng Geol*. 2018;243:218-230.
21. Singh A, Rao KS, Ayothiraman R. A closed-form analytical solution for circular opening in rocks using drucker–prager criterion. *Indian Geotech J*. 2019;49(4):437-454.
22. Singh A, Rao KS, Ayothiraman R. An analytical solution for a circular wellbore using Mogi-Coulomb failure criterion. *J Rock Mech Geotech Eng*. 2019;11(6):1211-1230.
23. Rice JR, Cleary MP. Some basic stress diffusion solutions for fluid-saturated elastic porous media with compressible constituents. *Rev Geophys*. 1976;14(2):227-241.
24. Detournay E, Cheng AD. Poroelastic response of a borehole in a non-hydrostatic stress field. *Int J Rock Mech Min Sci Geomech Abstr*. 1988;25(3):171-182.
25. Bai M, Roegiers JC. Fluid flow and heat flow in deformable fractured porous media. *Int J Eng Sci*. 1994;32(10):1615-1633.
26. Wang Y, Dusseault MB. Borehole yield and hydraulic fracture initiation in poorly consolidated rock strata—Part II. Permeable media. *Int J Rock Mech Min Sci Geomech Abstr*. 1991;28(4):247-260.
27. Han G, Dusseault MB. Description of fluid flow around a wellbore with stress-dependent porosity and permeability. *J Pet Sci Eng*. 2003;40(1-2):1-16.
28. Masoudian MS, Hashemi MA. Analytical solution of a circular opening in an axisymmetric elastic-brittle-plastic swelling rock. *J Nat Gas Sci Eng*. 2016;35:483-496.
29. Masoudian MS, Hashemi MA, Tasalloti A, Marshall AM. Elastic–brittle–plastic behaviour of shale reservoirs and its implications on fracture permeability variation: an analytical approach. *Rock Mech Rock Eng*. 2018;51:1565-1582.
30. Bernabe Y, Fryer DT, Shively RM. Experimental observations of the elastic and inelastic behavior of porous sandstones. *Geophys J Int*. 1994;117:403-418.
31. Hol S, Mossop AP, van der Linden AJ, Zuiderwijk PMM, Makurat AH. Long-term compaction behavior of Permian sandstones—An investigation into the mechanisms of subsidence in the Dutch Wadden Sea. Paper presented at: 49th US Rock Mechanics/Geomechanics Symposium. 2015; San Francisco, USA.
32. Hol S, van der Linden A, Bierman S, Marcelis F, Makurat A. Rock physical controls on production-induced compaction in the Groningen Field. *Sci Rep*. 2018;8:7156.
33. Pijnenburg RPJ, Verberne BA, Hangx SJT, Spiers CJ. Inelastic deformation of the Slochteren sandstone: stress-strain relations and implications for induced seismicity in the Groningen gas field. *J Geophys Res: Solid Earth*. 2019;124(5):1565-1582.
34. Pijnenburg RPJ, Verberne BA, Hangx SJT, Spiers CJ. Deformation behaviour of sandstones from the seismogenic Groningen gas field: role of inelastic versus elastic mechanisms. *J Geophys Res: Solid Earth*. 2018;123:5532-5558.
35. Wood MD. *Soil Behaviour and Critical State Soil Mechanics*. Cambridge, UK: Cambridge University Press; 1991.
36. Chen WF, Mizuno E. *Nonlinear Analysis in Soil Mechanics: Theory and Implementation*. Amsterdam, Netherlands; New York: Elsevier; 1990.
37. Li L, Li J, Sun DA, Gong W. Unified solution to drained expansion of a spherical cavity in clay and sand. *Int J Geomech*. 2017;17(8):04017028.
38. Mo P, Yu H. Drained cavity expansion analysis with a unified state parameter model for clay and sand. *Canadian Geotech J*. 2017;67:1-13.
39. Su D, Yang ZX. Drained analyses of cylindrical cavity expansion in sand incorporating a bounding-surface model with state-dependent dilatancy. *Appl Math Modell*. 2019;68:1-20.
40. Grant MA. Geothermal reservoir engineering. *Handbook of Clean Energy Systems*. 2015. https://doi.org/10.1002/9781118991978.hces103.
41. Fjaer E, Holt RM, Raaen AM, Risnes R, Horsrud P. *Petroleum Related Rock Mechanics*. Amsterdam; London: Elsevier; 2008.
42. Zhao Y, Borja RI. A continuum framework for coupled solid deformation–fluid flow through anisotropic elastoplastic porous media. *Comput Meth Appl Mech Eng*. 2020;369:113225.
43. Wang HF. *Theory of Linear Poroelasticity with Applications to Geomechanics and Hydrogeology*. Princeton, NJ: Princeton University Press; 2017.
44. Shampine LF, Kierzenka J. A BVP solver that controls residual and error. *J Numer Anal Ind Appl Math*. 2008;3:27-41.
45. Bai M, Elsworth D. Modeling of subsidence and stress-dependent hydraulic conductivity for intact and fractured porous media. *Rock Mech Rock Eng*. 1994;27(4):209-234.
46. Galin LA. Plane elastic-plastic problem: plastic regions around circular holes in plates. *Prikl Mat Mekh*. 1946;10:365-386.
47. Detournay E. An approximate statistical solution of the elastoplastic interface for the problem of Galin with a cohesive-frictional material. *Int J Solids Struct*. 1986;22(12):1435-1454.
48. Parisio F, Vilarrasa V, Wang W, Kolditz O, Nagel T. The risks of long-term re-injection in supercritical geothermal systems. *Nat Commun*. 2019a;10(1):1-11.
49. Wong TF. Effects of temperature and pressure on failure and post-failure behavior of Westerly granite. *Mech Mater*. 1982;1(1):3-17.

50. Ranjith PG, Viete DR, Chen BJ, Perera MSA. Transformation plasticity and the effect of temperature on the mechanical behaviour of Hawkesbury sandstone at atmospheric pressure. *Eng Geol*. 2012;151:120-127.
51. Shao S, Ranjith PG, Wasantha PLP, Chen BK. Experimental and numerical studies on the mechanical behaviour of Australian Strathbogie granite at high temperatures: an application to geothermal energy. *Geothermics*. 2015;54:96-108.
52. Parisio F, Vinciguerra S, Kolditz O, Nagel T. The brittle-ductile transition in active volcanoes. *Sci Rep*. 2019;9(1):143.
53. Misra AK, Murrell SAF. An experimental study of the effect of temperature and stress on the creep of rocks. *Geophys J Int*. 1965;9(5):509-535.
54. Semnani SJ, White JA, Borja RI. Thermoplasticity and strain localization in transversely isotropic materials based on anisotropic critical state plasticity. *Int J Numer Anal Methods Geomech*. 2016;40(18):2423-2449.
55. Bubshait A, Jha B. Coupled poromechanics-damage mechanics modeling of fracturing during injection in brittle rocks. *Int J Numer Methods Eng*. 2020;121(2):256-276.
56. Borja RI, Yin Q, Zhao Y. Cam-Clay plasticity. Part IX: on the anisotropy, heterogeneity, and viscoplasticity of shale. *Comput Meth Appl Mech Eng*. 2020;360:112695.

How to cite this article: Singh A, Fokker PA. Time-resolved model for geothermal engineering in high porosity Slochteren sandstone. *Int J Numer Anal Methods Geomech*. 2021;45:893–911. https://doi.org/10.1002/nag.3181